Optimization of fuel injection parameters of moringa oleifera biodiesel-diesel blend for engine-out-responses improvements

Yew Heng Teoh, Heoy Geok How, Farooq Sher, Thanh Danh Le, Hwai Chyuan Ong, Huu Tho Nguyen, and Haseeb Yaqoob

Original citation & hyperlink:
Teoh, Y.H., How, H.G., Sher, F., Le, T.D., Ong, H.C., Nguyen, H.T. and Yaqoob, H., 2021. Optimization of Fuel Injection Parameters of Moringa oleifera Biodiesel-Diesel Blend for Engine-Out-Responses Improvements. *Symmetry*, *13*(6), 982.
https://dx.doi.org/10.3390/sym13060982

DOI 10.3390/sym13060982
ISSN 2073-8994

Publisher: MDPI

symmetry

MDPI

Article

Optimization of Fuel Injection Parameters of *Moringa oleifera* Biodiesel-Diesel Blend for Engine-Out-Responses Improvements

Yew Heng Teoh [1,*], Heoy Geok How [2], Farooq Sher [3,*], Thanh Danh Le [4,*], Hwai Chyuan Ong [5], Huu Tho Nguyen [6] and Haseeb Yaqoob [1,7]

1 School of Mechanical Engineering, Engineering Campus, Universiti Sains Malaysia, Nibong Tebal 14300, Penang, Malaysia; haseeb.yaqoob@student.usm.my
2 Department of Engineering, School of Engineering, Computing and Built Environment, UOW Malaysia KDU Penang University College, 32, Jalan Anson, Georgetown 10400, Penang, Malaysia; heoygeok.how@kdupg.edu.my
3 Faculty of Engineering, Environmental and Computing, School of Mechanical, Aerospace and Automotive Engineering, Coventry University, Coventry CV1 5FB, UK
4 Faculty of Mechanical Engineering, Industrial University of Ho Chi Minh City, 12 Nguyen Van Bao Street, Ward 4, Go Vap District, Ho Chi Minh City 71408, Vietnam
5 School of Information, Systems and Modelling, Faculty of Engineering and IT, University of Technology Sydney, Ultimo, NSW 2007, Australia; ong1983@yahoo.com
6 Department of Fundamentals of Mechanical Engineering, Faculty of Automotive, Mechanical, Electrical and Electronic Engineering (FAME), An Phu Dong Campus, Nguyen Tat Thanh University, 331 National Route 1A, An Phu Dong Ward, District 12, Ho Chi Minh City 729800, Vietnam; nhtho@ntt.edu.vn or nguyenhuutho99@gmail.com
7 Department of Mechanical Engineering, Khwaja Fareed University of Engineering and Information Technology, Rahim Yar Khan 64200, Pakistan
* Correspondence: yewhengteoh@usm.my (Y.H.T.); Farooq.Sher@coventry.ac.uk or Farooq.Sher@gmail.com (F.S.); lethanhdanh@iuh.edu.vn (T.D.L.)

check for updates

Citation: Teoh, Y.H.; How, H.G.; Sher, F.; Le, T.D.; Ong, H.C.; Nguyen, H.T.; Yaqoob, H. Optimization of Fuel Injection Parameters of *Moringa oleifera* Biodiesel-Diesel Blend for Engine-Out-Responses Improvements. *Symmetry* **2021**, *13*, 982. https://doi.org/10.3390/sym13060982

Academic Editors: Sabino Armenise, Franck Launay and Marta Muñoz

Received: 23 April 2021
Accepted: 14 May 2021
Published: 1 June 2021

Publisher's Note: MDPI stays neutral with regard to jurisdictional claims in published maps and institutional affiliations.

Abstract: Biodiesel has gained popularity in diesel engines as a result of the rapid decline of fossil fuels and population growth. The processing of biodiesel from non-edible Moringa Oleifera was investigated using a single-step transesterification technique. Both fuels had their key physicochemical properties measured and investigated. In a common-rail diesel engine, the effects of MB50 fuel blend on the symmetric characteristics of engine-out responses were evaluated under five load settings and at 1000 rpm. As compared to standard diesel, MB50 increased brake thermal efficiency (BTE), and nitrogen oxides (NO_x) emissions while lowering brake specific fuel consumption (BSFC), and smoke emissions for all engine loads. A further study of injection pressure and start of injection (SOI) timing for MB50 fuel was optimized using response surface methodology (RSM). The RSM optimization resulted in improved combustion dynamics due to symmetry operating parameters, resulting in a simultaneous decrease in NO_x and smoke emissions without sacrificing BTE. RSM is an efficient optimization method for achieving optimal fuel injection parameter settings, as can be deduced. As a result, a clearer understanding of the use of MB50 fuel in diesel engines can be given, allowing for the best possible engine efficiency.

Keywords: renewable fuels; moringa biodiesel; common-rail; combustion; optimization; alternative fuel; response surface methodology; sustainability

1. Introduction

The exponential growth in the global population has caused a boom in energy demand, resulting in global energy supply crisis. This insufficiency will adversely impact the energy-dependent global economy. There is no doubt that fossil fuel was known as the main source of energy generation for many years. Unfortunately, these fossil fuels are non-renewable

resources that have a limited supply. Therefore, the production of fossil fuels is becoming one of the most prominent challenges in the imminent future, particularly to meet the future demand in transport application [1]. This has prompted a search for renewable and environmentally friendly alternative energy sources.

Over the past few months, the COVID-19 pandemic outbreak has significantly impacted all aspects of life, including the energy sector [2]. Despite this crisis, the worldwide renewable energy demand is expected to continue rise, albeit at a steadily lower rate, according to the IEA [3]. Owing to the diminishing rate of fossil fuel supplies and its many benefits, biodiesel has recently received a lot of publicity [4–6]. Biodiesel use is expected to reduce dependence on fossil fuels while also speeding up renewable energy transformations. Nevertheless, the extensive utilization of food-based crops for fuel production may cause another significant problem of food versus fuel competition. Accordingly, there is an immediate demand for alternative, sustainable fuels, and feedstocks to substitute food-based feedstocks. For the past few years, several researches [7–10] discovered that Moringa oleifera seed oil had given promising results as a non-edible feedstock in biodiesel production. The oil is regarded as non-edible oil and therefore oil extraction for biodiesel production becomes one of the foremost biofuel option to mitigate the on-going argument of food versus fuel crisis [11,12]. Moreover, since the oil does not clash with the available edible feedstock, which is mostly used as a food supply, it does not use additional land or impact food prices [13,14].

Recently, biodiesel production from non-food sources such as Moringa oleifera have drawn many researcher's attention, and most of them were focused on the application of this fuel in existing unmodified diesel engines [15–20]. Recently, Teoh et al. [18] reported the effect of utilization of symmetric blend of Moringa Oil Biodiesel (MB) and baseline diesel fuel on particulate matter emission and brake thermal efficiency in an unmodified diesel engine. Besides, another study performed by Mofijur et al. [21] to compare the physiochemical properties and engine performance of MB in a single-cylinder unmodified diesel engine. According to research, MB fuel has comparable performance to palm biodiesel and emits less pollutants than diesel fuel. Aside from that, the MB was found to have high thermo-oxidative stability, indicating that it is resistant to oxidative degradation [8,10,22].

Optimization was typically carried out in the parameter analysis in diesel engines using a multi-objective optimization approach containing multiple goals, such as minimizing brake specific fuel consumption (BSFC), nitrogen dioxide (NO_x), and smoke emissions while optimizing brake thermal efficiency (BTE). The injection parameters of a modern common rail fuel injection system can be modified to improve diesel engine efficiency and emissions. These injection parameters include injection timing, injection pressure, and split injection scheme. Nevertheless, the most significant parameter for tuning is injection timing. Different combustion and performance features will be created by the difference in start of injection (SOI) and injection length. Various experiments have shown that retardation of injection timing decreases NO_x pollution [23–26]. This was because by delaying the injection timing, the average combustion temperature and pressure in the cylinder were reduced, and hence the formation of NO_x was reduced. Ironically, with advanced injection timing, the emission of unburned hydrocarbon (HC) and carbon monoxide (CO) decreased. According to a report performed by Agarwal et al. [27] on the effect of fuel injection timing using fossil diesel on a single-cylinder diesel engine, advanced injection timing reduced HC and CO emissions while significantly increasing NO_x emissions. In diesel engines using a higher biodiesel blend (i.e., B50), injection parameters like injection fuel rail pressure and SOI timing can be adjusted to improve engine performance and fuel combustion. The optimization can be possibly performed using the technique of RSM. Conventionally, the optimization process has been carried out by varying a single factor and monitoring its impact on the result. The only disadvantage of this method is that it ignores the interactive effects of the tested variables. Multivariate statistical methods are, however, more favored. RSM is the most widely used multivariate technique in optimization. This technique has been widely used in a variety of engineering fields, including energy applications [28], the

food industry [29], analytical chemistry [30], and process and product optimization [31]. Yashvir Singh et al. [32] used RSM to increase the performance and emission parameters of pongamia methyl ester indirect injection diesel engines. The study found that by improving injection pressure, SOI timing, bio-diesel blends ratio, and engine load, the responses of engine BTE, HC, and NO_x emissions can be improved.

As the literature studies on the new non-edible biodiesel feedstock as a substitute for conventional diesel fuel in a common-rail direct-injection diesel engine are studied, it is found that there are not enough researches on the impact of edible biodiesel on engine performance and exhaust emissions. In addition, despite several prior studies reported on engine operation fueled with biodiesel blends in existing unmodified diesel engines, none of them referred to fuel injection parameters optimization particularly with a higher proportion of MB blend reaching the B50 level. As most of the countries have moved toward cleaner fuel and vehicles in the future, thus it is expected that high biodiesel blending levels will be regulated by the local government and this may raise concerns of fuel adaptability in exiting unmodified diesel engines. As a result, the innovation of this study is to use RSM as a systemic method to refine the fuel injection parameters of a common-rail diesel engine fueled by a high proportion of non-edible biodiesel blend fuel of MB50 (50% biodiesel, 50% petroleum diesel) in order to fill this research gap. Besides, another significant of this study is the employment of innovative radars plot of normalized results to effectively visual interpretation of data bearing multiple dimensions and subsequently helping researchers in making trade-off decisions.

2. Experimental Procedure and Design of Experiments

2.1. Experimental Procedure

The experiments in this study are run at a constant engine speed of 1000 rpm. The experiment program generally consists of two sets of studies to assess the effect of biodiesel on engine performance, combustion, and emission characteristics. Firstly, the experiment was performed with differing engine torque (i.e., 5, 10, 15, 20, and 25 Nm) while injection rail pressure and timing of injection were retained at constant stock values of 600 bar and 7°BTDC, respectively. The above five test points were selected as the most representative of a wide range of engine loads. For comparison purposes, diesel fuel was originally used as the reference fuel. Following that, a 50% volumetric proportion of diesel and methyl ester was measured. When fueled with MB50, the engine operates decently during the entire examination, which was conducted at room temperature of 25 °C and pressure of 1 atm, with no starting problems. Tests were conducted at a steady state along with a moderately warmed water coolant and temperature exhaust gas. Each evaluation point was redone two times for the calculation of average results.

As the engine was initially designed for diesel fuel, thus some optimization on injection parameters has to be carried out for engine operating with MB50 so that the engine performance is not affected by meeting emissions requirements or vice-versa when it fueled with MB50. Various fuel injection parameters have been identified to have a significant effect on BSFC, BTE, NO_x, and smoke emission, thus they must be carefully optimized when operating with MB50. The input factor of fuel injection parameters that vary during the latter part of the experiments are engine torque setting, fuel injection pressures (FIP), and fuel injection timings. A custom-made programmable engine control unit (ECU) was used to precisely control injection variables such as SOI timing, injection time, and FIP.

2.2. Design of Experiments

In this study, the RSM, which is a feature available in Design-Expert®® software (Stat-Ease Inc., Minneapolis, MN, USA), is adopted to analyze the interaction results between the engine-out responses and the input variables. A typical RSM design tool called Central Composite Design (CCD) is considered to investigate the influence of variation of injection parameters on engine-out responses. Three independent variables are A: Torque setting (10–20 Nm), B: SOI timing (5–9°BTDC), and C: FIP (400–800 bars). There are four critical

responses chosen, and it consists of BSFC, BTE, NO_x, and Smoke. The ranges and degrees of independent parameters studied are listed, as shown in Table 1, along with actual and coded levels of each variable. This present research fixed the α value at 1.68, which is the span of the axial point from the center that enables the design to rotate. Each design variable was examined at five separate coded stages (i.e., −1.68, −1, 0, 1, 1.68).

Table 1. Levels of the injection parameters and torque conditions.

Variables	Coding	Units	Actual Values for the Coded Levels				
			$-\alpha$ (−1.68)	−1	0	+1	$+\alpha$ (+1.68)
Torque Setting	A	Nm	6.59	10	15	20	23.41
SOI	B	°BTDC	3.625	5	7	9	10.38
FIP	C	bar	264	400	600	800	936

2.3. Statistical Analysis and Response Surface Optimization

The experimental results attained from CCD were evaluated by applying RSM. In the optimization stage, the experimental reaction can be evaluated using second-order polynomial as expressed in Equation (1).

$$y_{\text{pred}} = \beta_o + \sum_i^k \beta_i x_i + \sum_i^k \beta_{ii} x_i^2 + \sum_i^{k-1} \sum_{j=i+1}^k \beta_{ij} x_i x_j + \varepsilon \quad (1)$$

where y_{pred} are the predicted variables, x_i and x_j are the independent variables, β_o is the coefficient of constant, β_i, β_{ii}, and β_{ij} are the interaction coefficients of linear, quadratic, and second-order terms, respectively, and ε is the error. Regarding the fitting of the response surfaces, the models' level of fit was assessed using coefficients of determination (R^2), and the coefficient regression relevant (analysis of variances (ANOVA)) was validated using Fisher's test (F-test) [33]. After verification, these models were adopted for later evaluation of result and lastly for optimization.

2.4. Setup of Engine Testbed and Instrumentation

Figure 1 presents the experimental setup and instrumentation system. The study's research engine is a modified single-cylinder compression ignition diesel engine with the specifications listed in Table 2. The author's previous work covered the major engine changes on this engine's fuel distribution mechanism, the test engine's dynamics, and the overall test configuration [34]. Injection timing phasing is one of the most effective ways to minimize NO_x emissions in diesel engines. In the olden days, mechanical fuel injection systems were initially incorporated with variable injection timing. Recently, as modern digitalization gaining more widespread use in diesel engine control, fuel injection controlled through electronics became the choice of realizing variable injection timing that delivers unparalleled flexibility in injection timings controls. The present study managed fuel injection parameters through a programmable microcontroller and interfacing with LabVIEW program. The control unit was designed to enable the modification of numerous main engine operation variables which includes the SOI timing, fuel rail pressure, injection event per cycle, and injection quantity.

Figure 1. Experimental setup and instrumentation system used in the study.

To apply torque and adjust the engine's rpm, an A.C. synchronous dynamometer was used. A gear wheel flow meter was used to determine the rate of fuel consumption in the engine. The prototype engine had sensors for measuring symmetric combustion pressure and detecting fuel injection events. A Kistler 6125B style pressure sensor was used to determine the symmetric combustion chamber pressure, and the charge signal output from the sensor was processed with an in-line charge converter and signal conditioner. The rotational angle of the engine crankshaft was measured using a rotary shaft encoder of 720 pulses per revolution. The injector current measurement was quantified through the use of a Hall Effect current sensor in order to measure and validate the injection duration and SOI timing for the injector.

Table 2. Specifications of single-cylinder engine.

Parameter	Units	Values
Displacement	cm^3	638
Bore	mm	92
Stroke	mm	96
Compression ratio		17.7:1
Rated power	kW	7.8
Rated speed	rpm	2400
Combustion chamber		Re-entrant type

In addition, a computer with a high-speed simultaneous sampling data acquisition system with a sampling rate of 2 MS/s, a resolution of 14 bits, and four analogue input channels are used to acquire signals on cylinder friction, injector current and encoder at the same time. Matlab software was used to further processes and analyze the received data. For every test, pressure data from 100 combustion cycles were obtained, and the averaged was computed. Matlab programming was utilized to process the combustion information, namely location of peak pressure and heat release rate (HRR), ignition delay, rate of heat

release, and peak pressure magnitude. An AVL DICOM 4000 gas analyzer and an AVL DiSmoke 4000 were used to test NO_x concentration and smoke opacity, respectively, in terms of exhaust parameters. Table 3 shows the resolution and measurement range of both instruments.

Table 3. Measurement specifications of the gas and smoke analyzer.

Analyzer	Measurement Technique	Element	Measurement Range	Resolution
Gas analyzer	Electrochemical	Nitrogen oxides (NO_x, ppm)	0–5000	1
Smoke opacimeter	Photodiode detector	Opacity (%)	0–100	0.1

2.5. Methods of Calculation and Formula

In this study, the symmetric characteristics of engine performance of BSFC and BTE were evaluated and calculated by using Equations (2) and (3).

$$\text{BSFC (g/kWhr)} = \frac{\text{Fuel Consumption}}{\text{Brake Power}} \quad (2)$$

$$\text{BTE (\%)} = \frac{\text{Brake Power } \times 100}{\text{Calorific Value} \times \text{Fuel Consumption}} \quad (3)$$

For the combustion analysis, the HRR results were used to evaluate the impacts of engine operating conditions, engine design changes, fuel type, and fuel injection system on the engine efficiency and combustion process [35]. The HRR ($\frac{dQ}{d\theta}$) calculations based on the first law of thermodynamics could be calculated with the following Equation (4).

$$\frac{dQ}{d\theta} = \frac{\gamma}{\gamma - 1} P \frac{dV}{d\theta} + \frac{1}{\gamma - 1} V \frac{dP}{d\theta} \quad (4)$$

where γ = specific heat ratio, P = instantaneous cylinder pressure (Pa), and V = instantaneous cylinder volume (m^3).

3. Results and Discussion

3.1. Test Fuels and Fuel Properties Analysis

The fossil diesel fuel and Moringa Oleifera oil used in this study were obtained from a local Malaysian supplier. In general, there are many methods to convert vegetable oil into biodiesel, namely transesterification, microemulsion, dilution, and pyrolysis [36]. Nonetheless, the transesterification process remains the most popular and economical method [37]. As a result, this method has been commonly used to reduce the viscosity of crude vegetable oil as well as to extract ester and glycerol from triglycerides. In this study, transesterification along with the related post-treatment (purification and drying) processes is considered for the conversion of oil to MB and the steps involved are sequentially explained below.

In this study, the esterification process is not required for pre-treatment of the oil because of the considerably low acid value (about 5–10 mg KOH/gm). Before starting the transesterification process, a measuring cylinder and density meter were used to carefully measure the volume and density of crude Moringa Oleifera oil, respectively. The oil was then moved to a jacketed reactor, where the temperature was held at 60 °C with the aid of a heating circulator water tank. Then, once the catalyst is fully dissolved, methanol (9:1 methanol to oil ratio) and alkali catalyst (1 percent wt. KOH) are combined homogeneously. The mixtures were then applied to the preheated esterified oil before being stirred for 2 h with an overhead electric motor stirrer at a constant speed of 800 rpm. During the stirring operation, the reactor's temperature was kept at 60 °C. The fatty acid methyl ester (FAME) was carefully washed with purified water at 40 °C to remove impurities during

step separation of glycerol. Under standard room conditions, the blend was left to settle in a separated funnel for 2 to 3 h. The layer at the bottom, which is made up of impurities, was extracted out and discarded. Finally, the liquid was evaporated at 65 °C for 30 min to clear the excess methanol and water using a rotary evaporator.

Table 4 illustrated the details on the primary physicochemical properties of the converted neat MB relative to ASTM D6751 standard, in addition to the key properties of MB50 and petroleum diesel. It seems that MB's physicochemical properties are adequate to conform with ASTM biodiesel requirements. In fact, a remarkable improvement was observed for the kinematic viscosity of the transesterified Moringa Oleifera oil. However, it is marginally higher than petroleum diesel. Moreover, the resultant MB flash point was comparatively higher relative to petroleum diesel and are ideal for transportation fuel use. Still, the MB calorific value is lower compared to that of conventional diesel. The cetane number of fuels is another main feature that greatly affects the engine efficiency, combustion, and emissions characteristics. It is found that MB has a greater cetane number relative to petroleum fuels. A single diesel-MB blend, MB50 (50% biodiesel + 50% petroleum diesel) by volume, is considered and tested in a common-rail direct injection diesel engine in this analysis. In general, biodiesel can be used in a diesel engine either alone or in combination with petroleum diesel. In this report, higher blends of up to 50% are considered because they provide a reasonable combination of engine efficiency, emissions, production cost, cold-weather performance, and materials compatibility.

Table 4. The physicochemical properties of petroleum diesel, MB, and MB50 biodiesel blend.

Properties	Diesel Fuel	MB50	Biodiesel		MB
			Limit (ASTM D6751)	Test Method	
Kinematic viscosity @ 40 °C (mm^2/s)	3.34	4.05	1.9–6.0	D445	4.59
Density @ 15 °C (kg/m^3)	838.20	851.80	880	D127	885.50
Acid number (mg KOH/g)	0.12	0.180	<0.50	D664	0.24
Calorific value (MJ/kg)	45.31	42.11	-	D240	39.80
Flash point (°C)	71.5	98	>130	D93	189
Pour point (°C)	1	12	-	D2500	18
Cloud point (°C)	8	13	-	D2500	19
Oxidation stability @ 100 °C (h)	>100	25	>3	EN14112	6.50
Cetane number	52	55	>47	D6890	57

The fatty acid composition result for neat biodiesel is presented in Table 5. The oil was discovered to have a higher amount of unsaturated fatty acid (80.9 percent) relative to saturated fatty acid (19.1 percent). Fundamentally, the proportion of fatty acid content has a significant effect on biodiesel's physicochemical properties. A majority of non-edible oils consist of a higher degree of double carbon chain, which could influence the biodiesel's main properties, namely kinematic viscosity, the heat of combustion, oxidation stability, and cetane number [38]. In particular, the increase in carbon chain length could increase the calorific value, which dramatically modifies the biodiesel's cold properties [39]. Additionally, higher levels of unsaturated fatty acids will notably increase biodiesel's plugging points in the cold filter and its cloud point [40].

Table 5. Fatty acid composition of the biodiesel.

Sr. No.	Type	Fatty Acid Name (Systematic)	Systematic Name	MB (wt%)
1	Saturated fatty acid	C4:0 (Butyric)	Butanoic	0.50
2		C10:0 (Capric)	Decanoic	0.28
3		C12:0 (Lauric)	Dodecanoic	0.72
4		C14:0 (Myristic)	Tetradecanoic	0.45
5		C15:0 (Pentadecylic)	Pentadecanoic	12.26
6		C16:0 (Palmitic)	Hexadecanoic	0.50
7		C18:0 (Stearic)	Octadecanoic	4.39
8	Unsaturated fatty acid	C18:1n9c (Oleic)	(9Z)-Octadec-9-enoic acid	26.99
9		C18:2n6c (Linoleic)	(9Z,12Z)-9,12-Octadecadienoic acid	46.68
10		C18:3n6 (γ-linoleic)	all-cis-6,9,12-octadecatrienoic id	0.86
11		C18:3n3 (α-linolenic)	(9Z,12Z,15Z)-9,12,15-Octadecatrienoic	5.95
12		C20:3n6 (Dihomo-γ-linolenic)	cis,cis,cis-8,11,14-Eicosatrienoic	0.42
			Saturated fatty acid	19.10
			Unsaturated fatty acid	80.90
			Total	100.00

3.2. Engine-Out-Responses with Stock Setting

3.2.1. Engine Performance Analysis

Figure 2 presents the BSFC of the MB50 blended fuel and baseline diesel compared under various load conditions. The proportion of the fuel consumption rate to the brake power output is defined as BSFC. According to the findings, base-line diesel and MB50 have the lowest BSFC of 267.8 g/kWhr and 267.3 g/kWhr, respectively, at higher engine torque of 25 Nm. Furthermore, the overall pattern suggests that the MB50 blend consistently produced lower BSFC than the baseline diesel at all loading settings. A lower value in BSFC of MB50 indicates that lower fuel consumption is necessary to produce the equivalent level of power which is to be foreseen due to the better combustion performance of the MB50 relative to that of petroleum diesel.

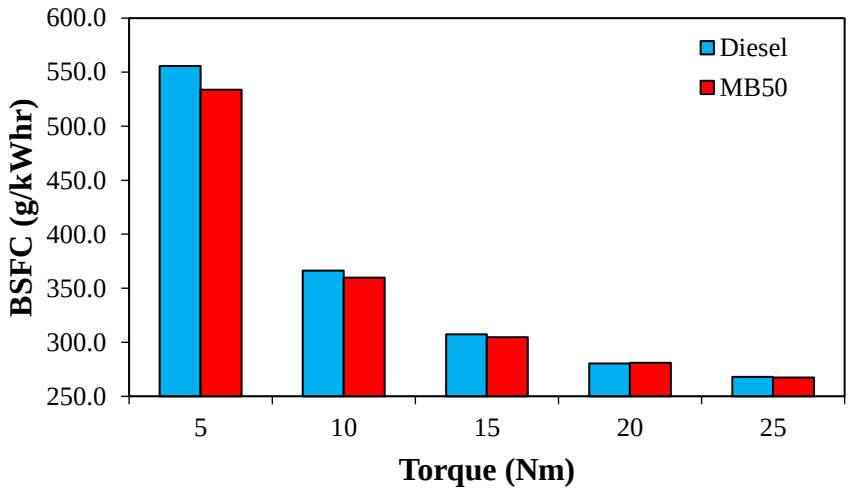

Figure 2. MB50 and diesel fuel's BSFC at different engine loads.

The BTE of an engine is a measure of its mechanical performance and net thermal efficiency. Similarly, BTE can be calculated by dividing the brake power output by the total energy input to the device. Owing to the effect of various failure causes, such as heat transfer, mechanical inertia, exhaust blowdown, combustion inefficiency, and flow, the BTE of an individual operating diesel cycle is typically below 50% and is often much lower [41]. The reduction of heat transfer is a large fraction of these losses, and it varies

with the average piston speed and the combustion properties of the fuel. Figure 3 shows the variation in BTE versus engine load for both fuel samples. As the engine load is increased, the BTE for both samples usually increases. This tendency can be attributed to the simultaneous effects of increased braking power and reduced wall heat loss as engine load increases [42,43]. Furthermore, for MB50, an average of 9% rise in BTE was observed overall in engine loads.

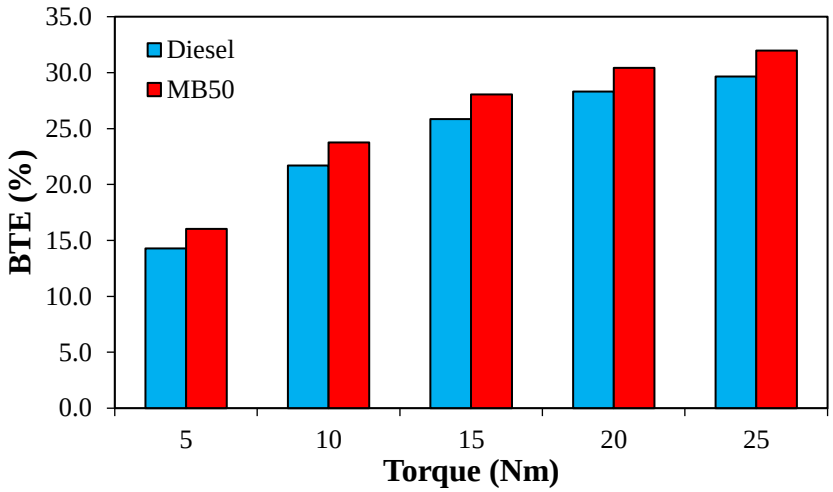

Figure 3. MB50 and diesel fuel's BTE at different engine loads.

3.2.2. Exhaust Emissions Analysis

NO_x formation of vehicle exhaust is largely determined by engine working conditions as well as the type and properties of the fuel [44]. The majority of research literature claims that using methyl ester blended gasoline increases NO_x emissions [45–47]. The explanations given are primarily based on the higher oxygen content, which results in a higher combustion temperature, which facilitates the formation of thermal NO_x. According to Figure 4, the NO_x generated by MB50 is higher than baseline diesel at all engine loads. The greatest increase recorded in NO_x formation was about 5.9% when the engine which was fueled with MB50 blend, operates at a load of 10 Nm. This increment can be associated with the comparatively higher content of MB50 fuel burned at mixing controlled and late combustion process and, subsequently, a higher average temperature of in-cylinder combustion [48,49]. Figure 5 depicts this effect. The graph shows the calculated in-cylinder combustion average temperature, injector current profile, and HRR of a 15 Nm engine using MB50 fuels and baseline diesel. As shown, an engine fueled with MB50 had a significant impact on the engine combustion characteristics that follows a pattern similar to the baseline diesel. It is found that MB50 fuel utilization gives off higher average combustion. Besides, the in-cylinder combustion temperature peak was shifted later toward the expansion stroke with the use of MB50 blend. The general combustion phases take place much later in the expansion stroke relative to those of baseline diesel which, in turn, enables the combustion yields to have longer residence time at high temperatures and raises the emission of NO_x. Another plausible explanation can be attributed to a drop in heat dissipation through radiation as a result of the significant decrement of soot produced from biodiesel use (see Figure 6), leading to higher NO_x formation [50].

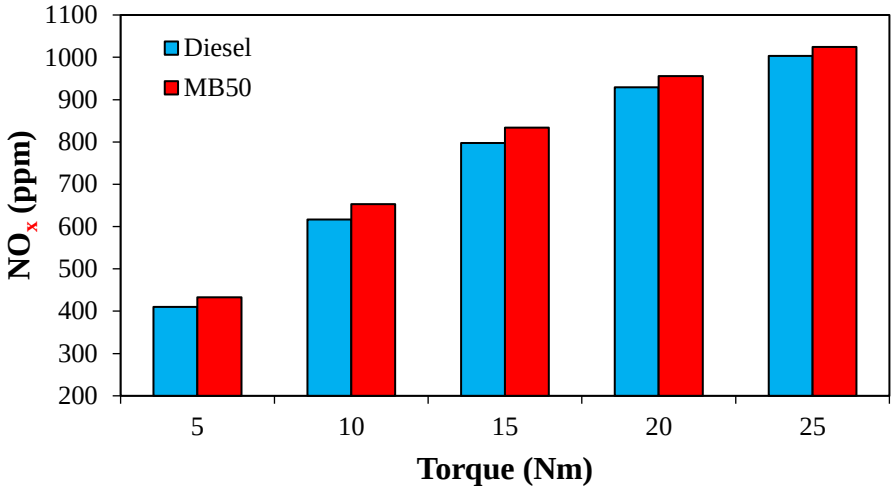

Figure 4. MB50 and diesel fuel's NO_x emission at different engine loads.

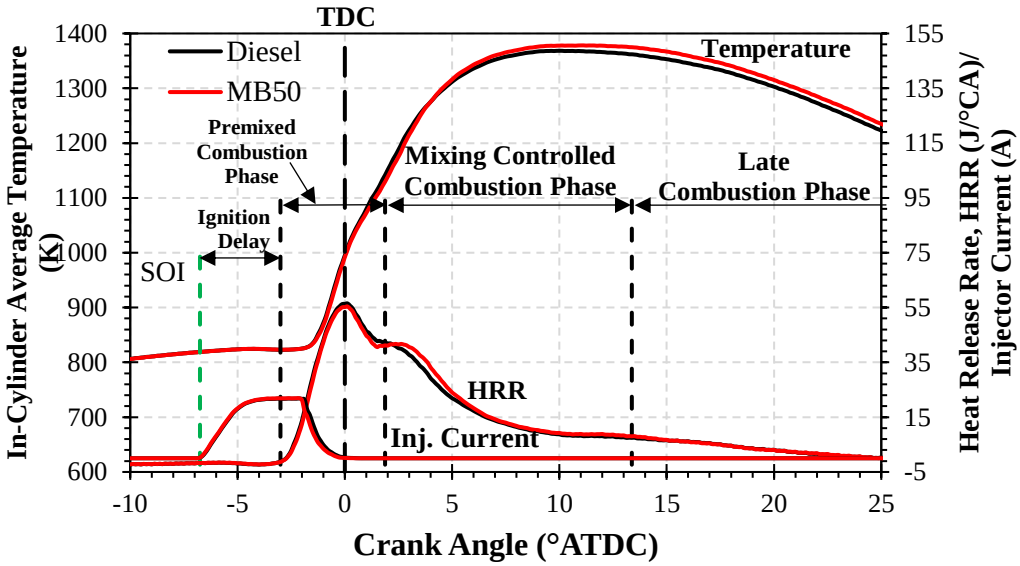

Figure 5. In-cylinder combustion average temperature, HRR, and injector current profiles for diesel and MB50 fuel at 15 Nm.

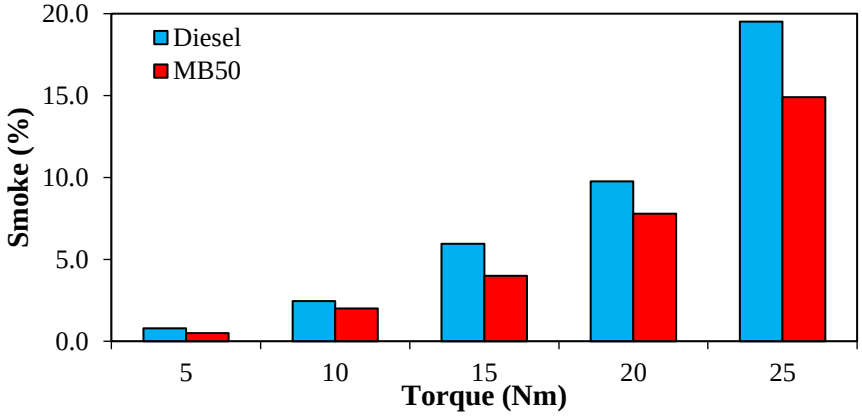

Figure 6. MB50 and diesel fuel's smoke emission at different engine loads.

Figure 6 depicts the opacity of smoke emission for each of the measured fuels. In terms of the effect of engine load on smoke opacity, it was discovered that as engine load

increases, the opacity level continues to rise. Furthermore, the smoke emissions of the MB50 are consistently smaller than those of the benchmark diesel for all engine loads. The maximum reduction with MB50 was 37.5 percent at a 5 Nm engine load, according to the researchers. The decreased opacity of smoke is thought to be due to the cumulative effects of lower sulphur, lower impurities, and higher oxygen content in methyl ester oils [42].

3.3. Response Surface Analysis

A second-order reaction surface model involving 19 experiments with MB50 was fitted using a five-level three-factor CCD, which consisted of 8 factorial points for the 5 replicates from 14 complete factorial design CCD, 6 axial points, and 3 parameters at the centre points. The five replicates at the design centre point were used to calculate the data reproducibility and the experimental error. Table 6 depicts the experiment matrix and the corresponding responses. The tests were performed randomly to reduce systematic errors of the variables.

Table 6. Experimental results of five replicates of the center points for the three independent variables for MB50 fuel.

Std. Order	Point Type	Coded Independent Variable Levels			Experimental Results of the Responses			
		A: Torque Setting (Nm)	B: SOI (°BTDC)	C: FIP (bar)	BSFC (g/kWhr)	BTE (%)	NO_x (ppm)	Smoke (%)
1	Fact	10 (−1)	5 (−1)	400 (−1)	364.2	23.5	413	2.2
2	Fact	20 (1)	5 (−1)	400 (−1)	282.5	30.3	530	6.2
3	Fact	10 (−1)	9 (1)	400 (−1)	356.9	24.0	637	1.8
4	Fact	20 (1)	9 (1)	400 (−1)	280.7	30.5	846	5.8
5	Fact	10 (−1)	5 (−1)	800 (1)	376.2	22.7	696	0.6
6	Fact	20 (1)	5 (−1)	800 (1)	293.9	29.1	993	5.4
7	Fact	10 (−1)	9 (1)	800 (1)	368.3	23.2	1037	1.1
8	Fact	20 (1)	9 (1)	800 (1)	285.7	29.9	1582	5.0
9	Axial	6.6 (−1.68)	7 (0)	600 (0)	457.1	18.7	400	1.4
10	Axial	23.4 (+1.68)	7 (0)	600 (0)	278.8	30.7	989	7.2
11	Axial	15 (0)	3.625 (−1.68)	600 (0)	316.5	27.0	573	3.9
12	Axial	15 (0)	10.375 (+1.68)	600 (0)	305.0	28.0	1222	3.2
13	Axial	15 (0)	7 (0)	265 (−1.68)	305.1	28.0	436	4.5
14	Axial	15 (0)	7 (0)	935 (+1.68)	318.8	26.8	1192	2.5
15	Center	15 (0)	7 (0)	600 (0)	311.7	27.4	839	3.0
16	Center	15 (0)	7 (0)	600 (0)	308.7	27.7	834	3.0
17	Center	15 (0)	7 (0)	600 (0)	309.4	27.6	850	3.1
18	Center	15 (0)	7 (0)	600 (0)	309.2	27.7	859	3.0
19	Center	15 (0)	7 (0)	600 (0)	310.3	27.6	856	3.1

3.3.1. Model Validation

The quadratic model was selected as the best match to the answer because it has the highest order polynomial, implying that additional terms and the model were not aliased. The model equations are expressed with coded values (A: torque setting, B: SOI, and C: FIP) for the BSFC, BTE, NO_x, and smoke were represented by Equations (5)–(8), respectively. Generally, the positive and negative signs before the terms indicate the synergistic and antagonistic effects in the increment of responses, respectively [51]. For reference, the model of Equation (5) showed that when coefficients of C is positive, A^2 and AB reflected a linear effect to raise the BSFC. However, other terms of A, B, B^2, C^2, AC, and BC had counter effects that drop the BSFC value.

$$BSFC = 310.05 - 45.59A - 3.25B + 4.61C + 19.38A^2 - 0.82B^2 - 0.41C^2 + 0.67AB - 0.88AC - 0.88BC. \quad (5)$$

$$BTE = 27.59 + 3.40A + 0.27B - 0.38C - 0.99A^2 + 0.01B^2 - 0.03C^2 + 0.01AB - 0.03AC + 0.08BC. \quad (6)$$

$$NO_x = 845.71 + 158.16A + 187.60B + 230.86C - 44.99A^2 + 26.83B^2 - 2.67C^2 + 42.52AB + 64.42AC + 48.74BC. \quad (7)$$

$$Smoke = 3.06 + 1.94A - 0.14B - 0.53C + 0.37A^2 + 0.11B^2 + 0.093C^2 - 0.11AB + 0.085AC + 0.12BC. \quad (8)$$

The relevance and fitness of the quadratic model, as well as the influence of relevant individual words and their association with the chosen responses, is statistically assessed

using an ANOVA. Table 7 contains a summary of the results. It should be noted that the *p*-value (probability of error value) is used to validate the importance of each regression coefficient, which represents the similarity of each cross-product. A lower *p*-value, for example, means that the related coefficient is more important [52]. In terms of the model, the *p*-value, which is less than 0.1 (outlined by the bold italic terms), statistically implies that the specific model terms were significant. As an example, from the ANOVA outcomes, the key model terms indicated that parameters with major effects on NO_x response are torque setting (A), SOI (B), FIP (C), and the correlation terms were discovered to be present between the key factors (AB, AC, and BC). In contrast, significant quadratic terms were torque setting (A^2) and SOI (B^2). A decrease in variation coefficient value (CV, 4.52%) implies an increase in precision and a high degree in the experimental values' reliability. Other than ANOVA, the precision index values, namely 'Adeq Precision', 'predicted R^2', and 'adjusted R^2', were also applied to validate model predictions' similarity to experimental data. The precision index values of various responses are listed in Table 8. 'Adeq Precision' determines the signal-to-noise ratio. Generally, the 'Adeq Precision' value, which is higher than 4, shows moderate accuracy in model prediction. The estimated values versus experimental values for BSFC, BTE, NO_x, and smoke with R^2 value are displayed in Figure 7. The estimated and actual values were in fair alignment (R^2 value approaching unity), indicating an acceptable data fit of the model and high credibility in predicting system response in the range tested.

Table 7. Various applied models and *p*-values by ANOVA.

Model Terms	*p*-Value			
	BSFC	**BTE**	**NO_x**	**Smoke**
Model	Quadratic	Quadratic	Quadratic	Quadratic
F-value (*p*-value)	53.75 (<0.0001)	418.99 (<0.0001)	130.93 (<0.0001)	60.31 (<0.0001)
A	*<0.0001*	*<0.0001*	*<0.0001*	*<0.0001*
B	0.1876	*0.0012*	*<0.0001*	0.1451
C	*0.0737*	*0.0001*	*<0.0001*	0.0002
A^2	*<0.0001*	*<0.0001*	*0.0017*	0.0023
B^2	0.7261	0.8928	*0.0269*	0.2317
C^2	0.8626	0.6503	0.7985	0.3204
AB	0.8275	0.94	*0.0108*	0.3653
AC	0.7748	0.7318	*0.0009*	0.4801
BC	0.7735	0.3117	*0.0051*	0.3447
Coefficient of variation	2.60	0.80	4.52	9.39
Lack of fit	0.0003	0.0448	0.0055	0.0007

Table 8. Precision index values of different responses.

Responses	Precision Index Values			
	R-Squared	**Adj R-Squared**	**Pred R-Squared**	**Adeq Precision**
BSFC	0.9817	0.9635	0.8622	26.9208
BTE	0.9976	0.9952	0.9830	73.7255
NO_x	0.9924	0.9848	0.9414	42.3535
Smoke	0.9837	0.9674	0.8748	27.583

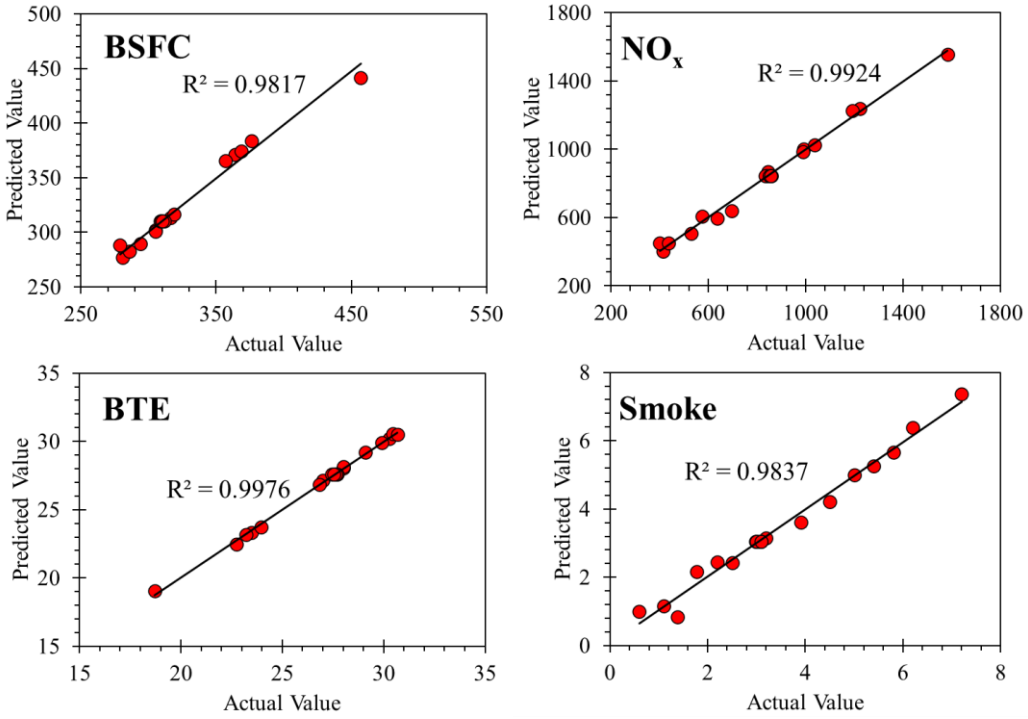

Figure 7. Predicted versus actual value of different responses.

3.3.2. BSFC Model

Figure 8a,b revealed the response surface plots for the correlation between SOI timing (B) and FIP (C) and the correlation between torque (A) and FIP (C), respectively, toward BSFC of the MB50 engine. At a fixed torque setting of 15 Nm, the results suggest that reduced BSFC can be attained by lowering the rail pressure and retarding the SOI timing. This can be explained by the gradually decreases in the effect of negative work during compression stroke with lower rail pressure and retarded SOI timing, therefore caused a decrease in the BSFC. Besides, observations made from response surface plots indicate that at fixed SOI timing 7°BTDC, the BSFC drops when the torque setting is incremented at any given rail pressure. This reduction in BSFC can be related to the continuous improvement in combustion quality and efficiency as the engine torque setting increases with constant rail pressure. Figure 9 presents the cylinder pressure and heat release rate curves for the engine operated with MB50, injection timing of 7°BTDC, the constant fuel injection pressure of 600 bar, and various torque settings. As can be seen, higher in-cylinder pressure is due to higher engine torque setting and injected fuel quantity, which burned more entirely and hence consumes less fuel for every unit of brake power.

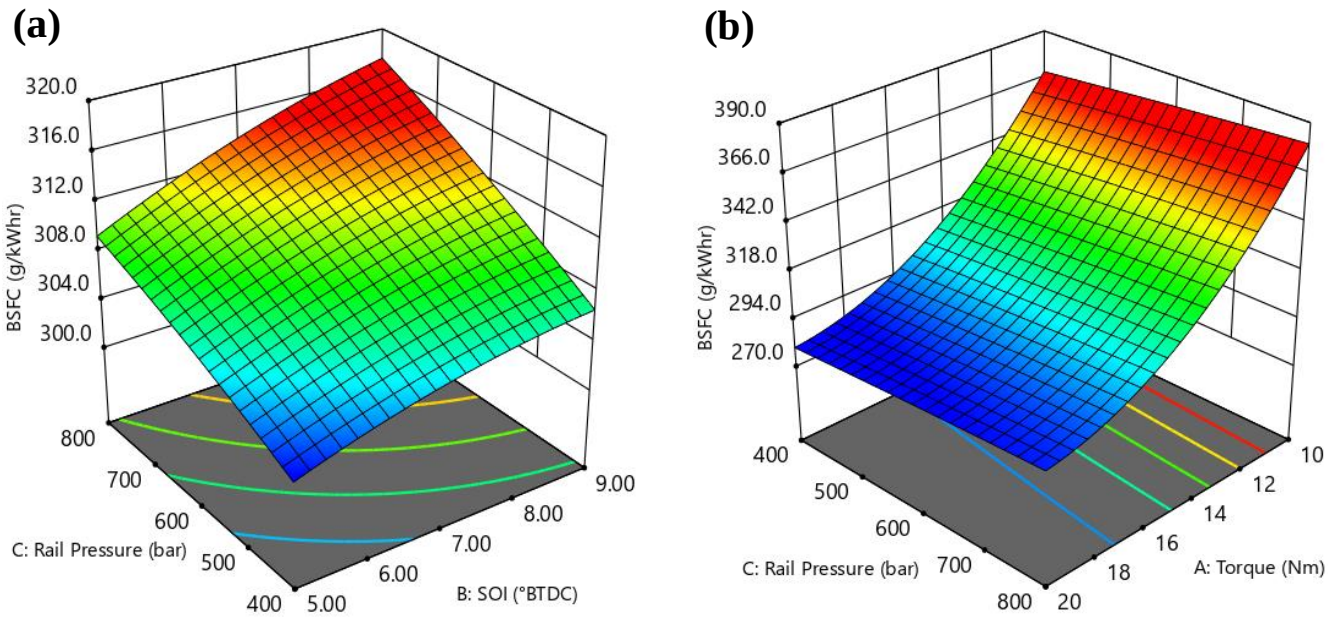

Figure 8. Response 3D surface plots for parameters interaction effect on BSFC; (**a**) Torque Setting: 15 Nm, (**b**) SOI: 7°BTDC.

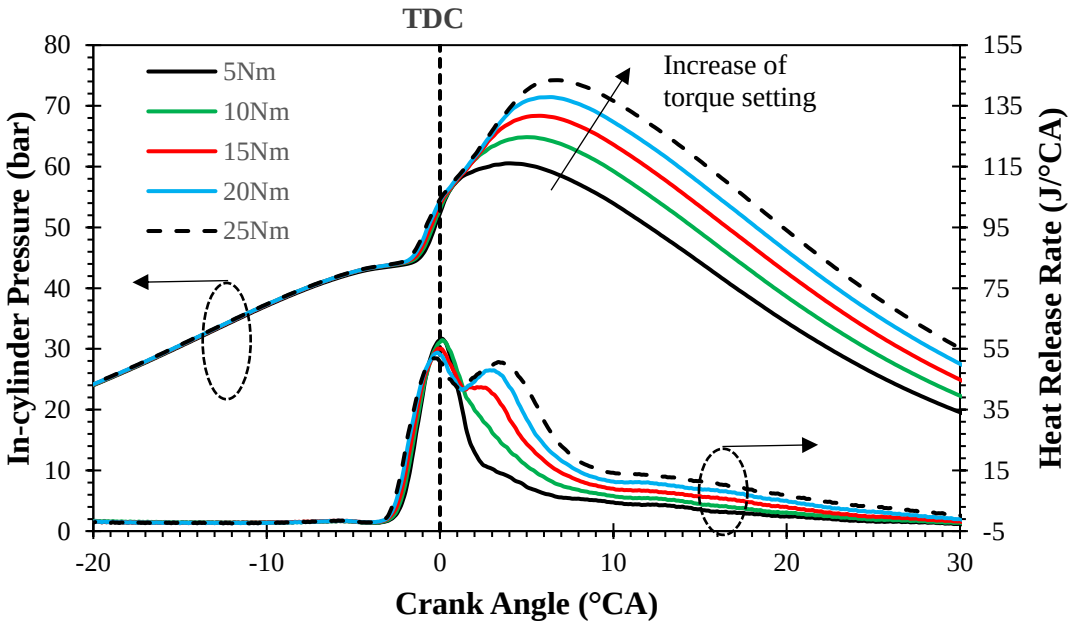

Figure 9. Combustion pressure and HRR for MB50 fuel with 7°BTDC of SOI, 600 bar of FIP, and at various torque setting.

3.3.3. BTE Model

Figure 10a,b revealed the response 3D surface plots for the correlation between SOI timing (B) and FIP (C) and the correlation between torque (A) and FIP (C), respectively, toward BTE of the MB50 engine. At a constant torque setting of 15 Nm, the results revealed that the SOI advancement from 5 to 9°BTDC leads to the decrease of BTE. Figure 11 indicates the variation of combustion pressure and HRR corresponding to the crank angle with different SOI timing at 600 bar. As can be seen, the combustion process coupled very well with the variation in SOI timing. Advancing SOI timing leads to higher pressure peak, and its location of occurrence also shifted near to the TDC position in the expansion stroke. Besides, at fixed SOI timing of 7°BTDC, the increase of torque setting has dramatically improved the BTE at any given rail pressure. Conversely, the increase of rail pressure does not significantly improve the BTE at all torque setting levels. Figure 12 demonstrates the

variation of combustion pressure and HRR corresponding to the crank angle for the engine operated with MB50, 15 Nm, stock SOI of 7°BTDC, and at various levels of FIP.

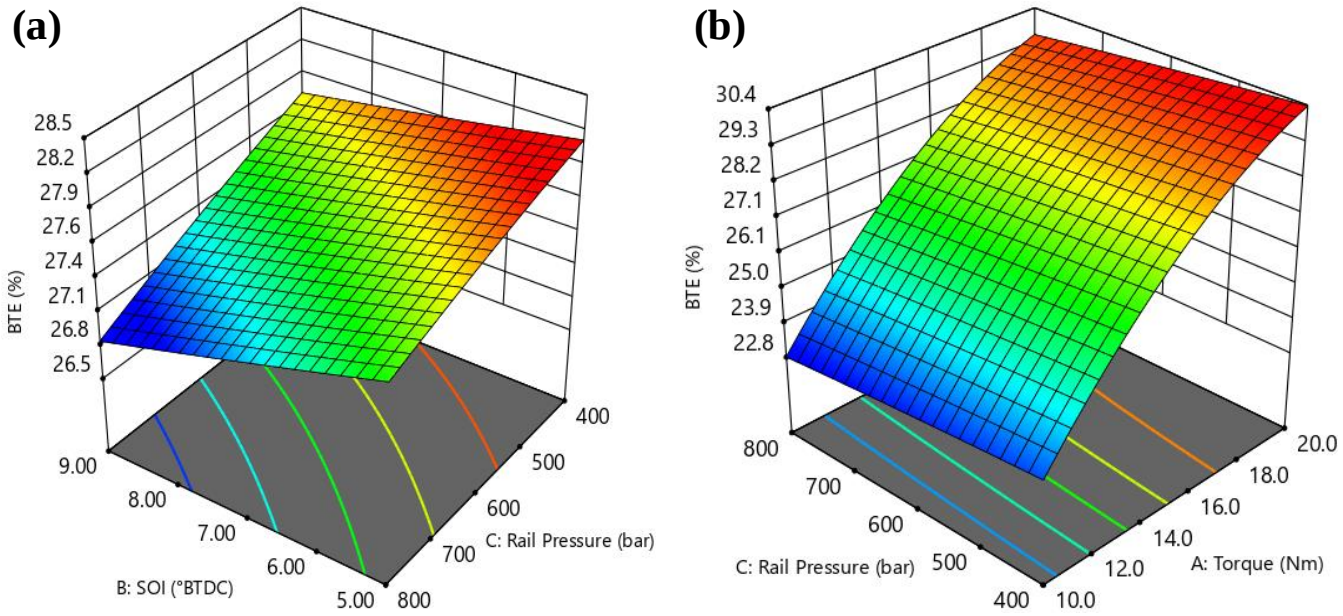

Figure 10. Three-dimensional response surface plots of BTE under; (**a**) Torque setting: 15 Nm, and (**b**) SOI: 7°BTDC.

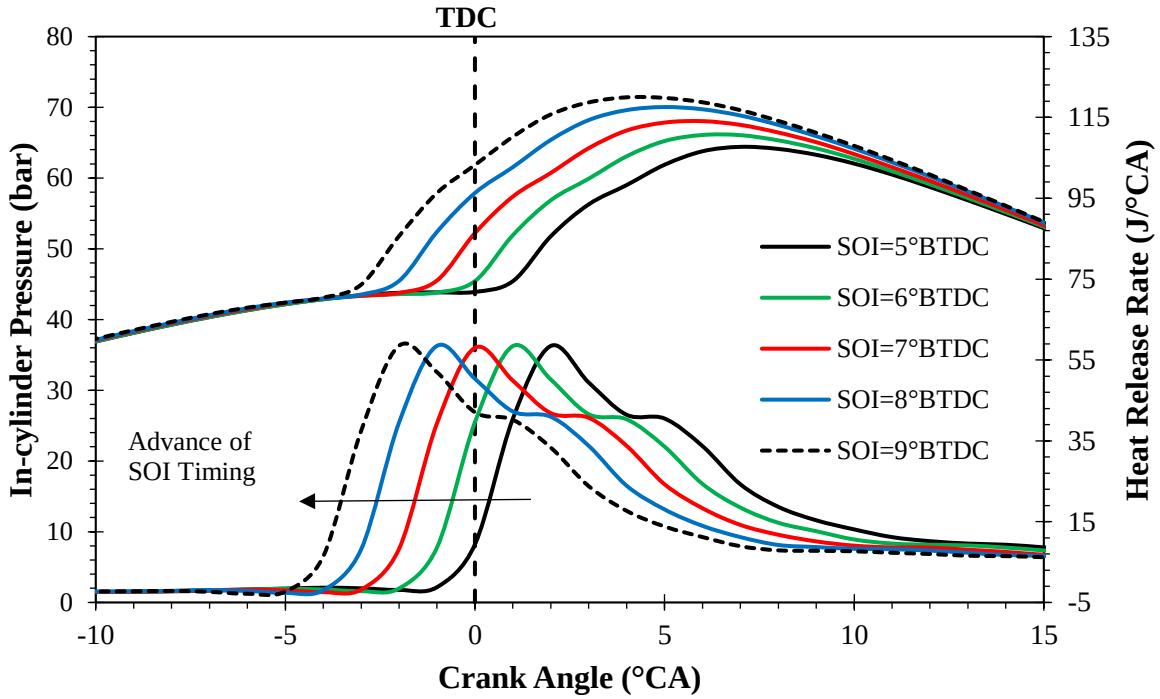

Figure 11. Combustion pressure and HRR for MB50 fuel, 15 Nm of torque, stock FIP of 600 bar, and at various SOI timings.

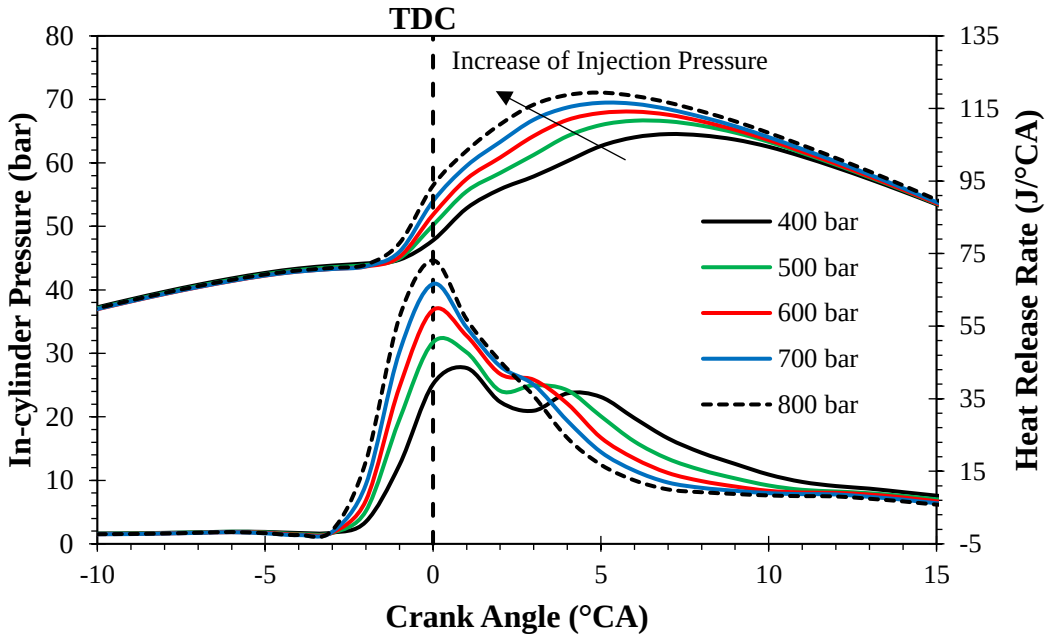

Figure 12. Combustion pressure and HRR for MB50 fuel, 15 Nm of torque, stock SOI of 7°BTDC, and at various levels of FIP.

3.3.4. NO_x Model

Figure 13a,b revealed the response 3D surface plots for the correlation between SOI timing (B) and FIP (C) and the correlation between torque (A) and FIP (C), respectively, toward NO_x of the MB50 engine. At a constant torque setting of 15 Nm, the results revealed that the advancement of SOI timing from 5°BTDC to 9°BTDC leads to the increase of NO_x. As aforementioned, advancing SOI timing leads to a higher pressure peak, and consequently increases the combustion temperature and NO_x emission. Besides, at fixed SOI timing of 7°BTDC, the increase of torque setting has dramatically increased the NO_x at any given rail pressure.

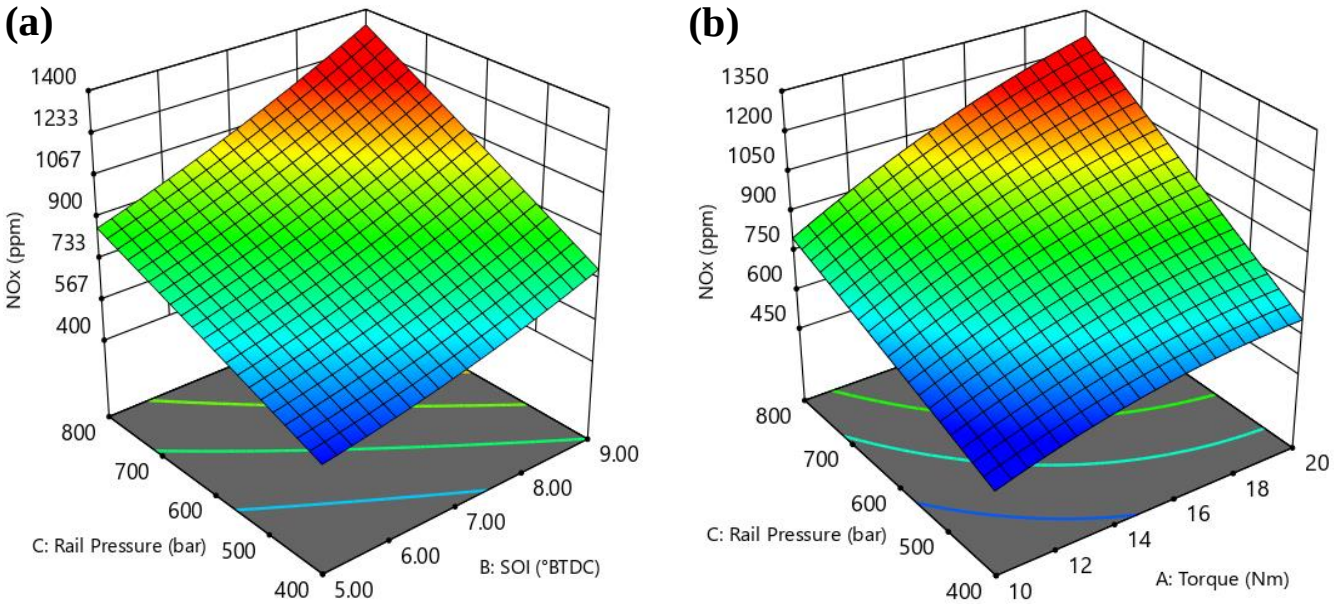

Figure 13. Three-dimensional response surface plots of NO_x under; (**a**) Torque setting: 15 Nm, and (**b**) SOI: 7°BTDC.

3.3.5. Smoke Model

Figure 14a,b revealed the response 3D surface plots for the correlation between SOI timing (B) and FIP (C) and the correlation between torque (A) and FIP (C), respectively, toward smoke emission of the MB50 engine. At a constant torque setting of 15 Nm, the results revealed that the advancement of SOI timing from 5°BTDC to 9°BTDC leads to the decrement of smoke. As aforementioned, advancing SOI timing leads to a higher pressure peak, and consequently increases the combustion temperature and enhanced fuel oxidation, which translated to the lower smoke emission. Besides, at fixed SOI timing of 7°BTDC, the increase of torque setting has dramatically increased the smoke at any given rail pressure.

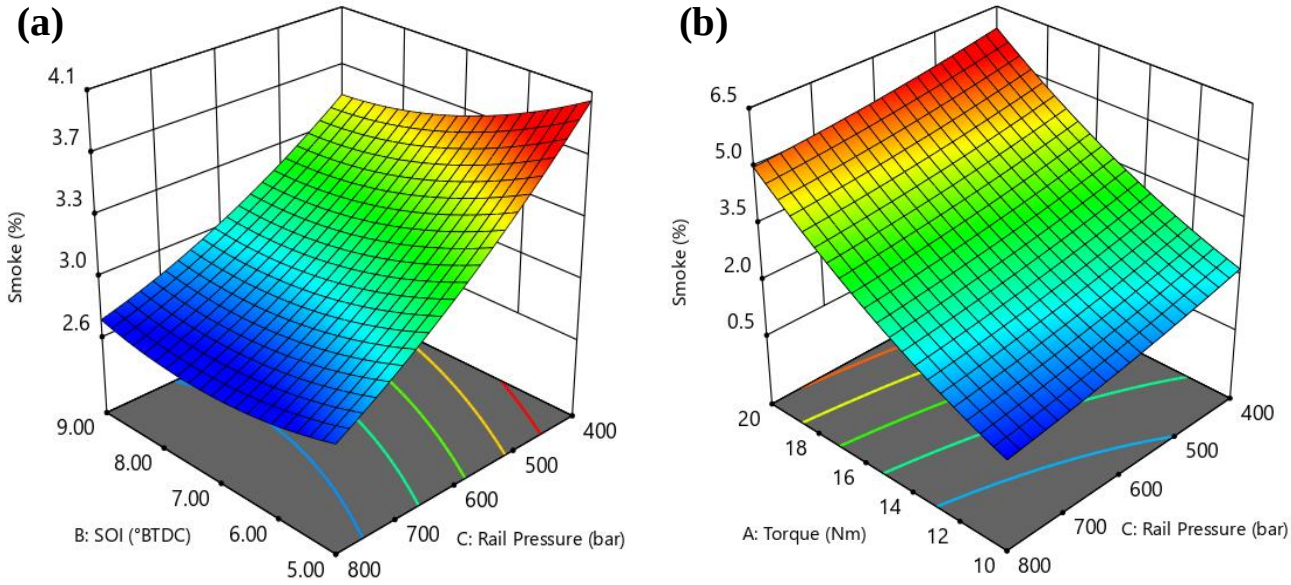

Figure 14. Three-dimensional response surface plots of smoke under; (**a**) Torque setting: 15 Nm, and (**b**) SOI: 7°BTDC.

3.4. Parameters Optimization and Experiment Results Validation

As there was a trade-off between BTE, BSFC, NO_x, and smoke, it was necessary to optimize the SOI and FIP at the corresponding torque setting to reduce NO_x and smoke and maximize the BTE without compromising BSFC. The prediction process for optimized engine operation is carried out by selecting the goal for each of the factor and response parameters. The desired goal could be set within the specified limits as a target, equal to, in-range, maximize and minimize. In this analysis, the optimization of engine operation with MB50 fuel was carried out in order to seek an optimal combination of operating conditions in which, under each torque setting, maximum BTE and minimum BSFC, NO_x, and smoke were achieved.

In this study, the desirability-based approach that is available in Design-Expert®® software was used to find the optimum setting. All goals are merged into one desirability function with several responses and factors, and the high desirability solution was preferred. As tabulated in Table 9 is the optimization of BSFC, BTE, NO_x dan smoke parameters for independent input variables of SOI and FIP at various engine torque settings. As can be seen, a very high desirability value of close to 1.0 is obtained for all cases. For each of the torque setting, a total of three optimum solutions were generated and compared, namely with optimized rail pressure, optimized SOI and optimized rail pressure and SOI. The first two conditions were set for optimizing of a single factor, while the latter is for optimizing two factors. These optimization results were then compared with the stock condition of SOI at 7°BTDC and FIP of 600 bar. Generally, the results revealed that the changes in BSFC and BTE are insignificant with the variation of input parameters of SOI and FIP at all torque settings. Besides, it can be seen that for each of the torque settings, the most optimistic response characteristics can be observed with optimization of the

dual factors of FIP and SOI. The results can be clearly seen with the radar plot of the normalized optimization for all torque settings, as shown in Figure 15. When the values of the optimized rail pressure and SOI solution are compared to the stock condition at higher torque of 20 Nm, the response obtained was higher performance levels at 30.6% of BTE and low BSFC of 277.2 g/kWhr, while emission levels were low at 506 ppm of NO_x and 5.2% of smoke opacity.

Table 9. Optimization results for 10, 15, and 20 Nm of torque settings.

Torque (Nm)	SOI (°BTDC)	Rail Pressure (bar)	BSFC (g/kWhr)	BTE (%)	NO_x (ppm)	Smoke (%)	Desirability	Remarks
10	7.000 [a]	600 [b]	366.0	23.6	653	2.0	-	Stock condition
	7.000 [a]	400	369.1	23.5	473	1.6	0.955	Optimized rail pressure
	5.000	600 [b]	370.3	23.5	524	1.5	0.954	Optimized SOI
	5.000	400	365.3	23.7	404	1.4	0.959	Optimized rail pressure and SOI
15	7.000 [a]	600 [b]	306.5	27.9	834	4.0	-	Stock condition
	7.000 [a]	400	305.0	27.9	612	3.5	0.973	Optimized rail pressure
	5.000	600 [b]	306.0	27.9	685	3.4	0.971	Optimized SOI
	5.000	400	301.9	28.1	500	3.3	0.977	Optimized rail pressure and SOI
20	7.000 [a]	600 [b]	282.6	30.3	955	7.8	-	Stock condition
	7.000 [a]	400	279.7	30.4	661	5.3	0.969	Optimized rail pressure
	5.000	600 [b]	280.4	30.3	756	5.3	0.966	Optimized SOI
	5.000	400	277.2	30.6	506	5.2	0.974	Optimized rail pressure and SOI

[a] Stock SOI timing; [b] Stock rail pressure setting.

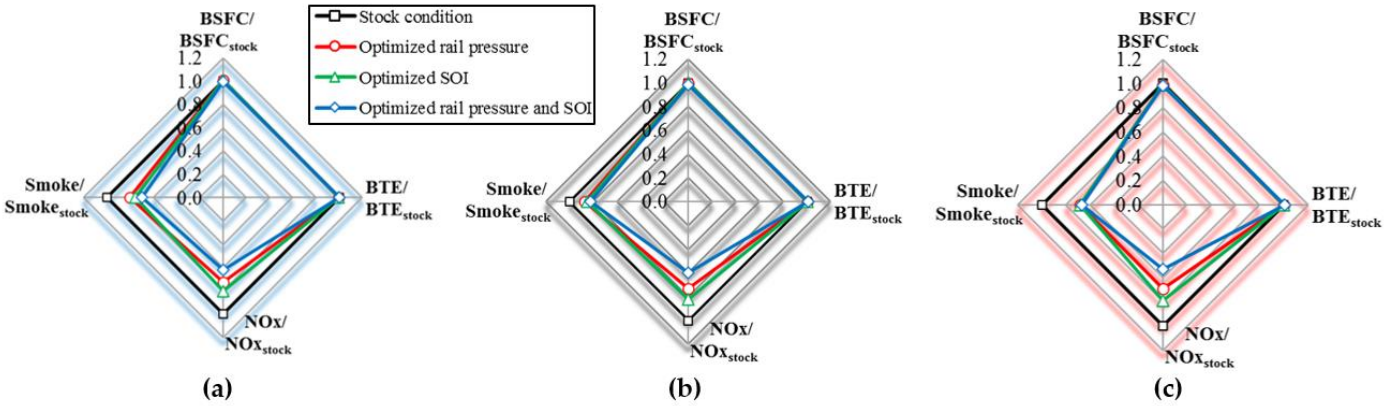

Figure 15. Radar plot of the normalized optimization results; (**a**) 10, (**b**) 15, and (**c**) 20 Nm of torque settings.

On the other hand, an experiment with optimized parameters was performed for the confirmation of optimization results and the outcome was compared to the predicted value. Shown in Table 10 are the experimental and predicted results. As can be seen, the percentage error between the experimental and predicted results for most of the parameters is less than 5%, except for the smoke result. Higher error for the smoke result can be associated with the considerably lower exhaust smoke level which is below the instrument detection limit and consequently results in a less stable measurement. Nevertheless, in general, the optimum parameters suggested by the software are acceptable. In addition, as shown in Table 11 is the comparison of engine out-responses for the optimized MB50 fuel and baseline diesel at 20 Nm. As aforementioned, the engine operating condition for baseline diesel is set at constant stock values of 600 bar and 7°BTDC. As can be seen, improvement results were obtained for BTE, NO_x and smoke, but with some deteriorating

in BSFC. This has demonstrated a simultaneous reduction in NO_x and smoke emissions can be obtained without sacrificing BTE. In fact, the highest reduction of 75.3% in NO_x emission was obtained for the optimized MB50 fuel as compared to the baseline diesel and this again demonstrated the effectiveness of the optimization approach used in this study.

Table 10. Comparison of experimental and predicted results under optimized rail pressure and SOI at 20 Nm.

Parameter	Experimental	Predicted	Error = $\frac{Experiment-Predict}{Experiment} \times 100\%$
BSFC (g/kWhr)	282.5	277.2	1.9%
BTE (%)	30.3	30.6	−1.0%
NO_x (ppm)	530	506	4.5%
Smoke (%)	6.2	5.2	16.1%

Table 11. Comparison of optimized MB50 fuel and baseline diesel at 20 Nm.

Parameter	MB50	Diesel	Changes (%)
BSFC (g/kWhr)	282.5	278.0	1.60
BTE (%)	30.3	28.7	5.30
NO_x (ppm)	530	929	−75.30
Smoke (%)	6.2	9.8	−58.10

4. Conclusions

It can be inferred from this analysis that the feasibility of Moringa Oleifera oil as a non-edible feedstock for biodiesel production is possible. In this study, using a single-step transesterification technique, biodiesel was successfully processed in the presence of base catalysts. Related to fossil diesel fuel, the physicochemical properties of the MB50 blend are found to be similar. The ASTM biodiesel requirements were met by all of the properties. Furthermore, the effects of the MB50 blend on engine efficiency, exhaust emissions, and combustion characteristics have been successfully assessed at 1000 rpm under different loads. A further analysis on the optimization of fuel injection parameters for MB50 fuel was optimized by using RSM. The SOI and FIP were included in the fuel injection parameters. The following key findings are summarized as follows:

- As compared to the baseline diesel fuel, the use of MB50 has improved the BSFC for engine service in stock conditions. Furthermore, the BTE of MB50 is consistently higher than that of baseline diesel in all load conditions.
- In terms of engine-out emissions, the NO_x emission for the MB50 fuel increased relative to that of baseline diesel across all engine loads. For the MB50 at 10 Nm, the largest increment in NO_x reported was around 5.9%. On the other hand, an improvement effect on the reduction of smoke emissions was observed with MB50 fuel across all engine loads.
- On the aspects of combustion, the MB50 fuel has produced higher in-cylinder combustion average temperature and the peak has shifted later toward the expansion stroke. This phenomenon has resulted in an extended residence period at high temperatures and raises the emission of NO_x.
- It can be inferred that RSM is an effective optimization approach for obtaining optimum fuel injection parameter settings for adaptation of MB50 fuel in a common rail injection diesel engine. The RSM optimization led optimum operating parameters in improving combustion characteristics, resulting in a simultaneous reduction in NO_x and smoke emissions without compromising BTE. With MB50 fuel, the highest NO_x reduction of 75.3% can be obtained with optimum fuel injection parameter settings.
- The most optimistic response characteristics has been attained with optimization of the dual factors of FIP and SOI. The optimum injection parameters to achieve higher performance levels and cleaner exhaust emissions has been obtained with retarded SOI of 5°BTDC and 400 bar of injection rail pressure. Besides, the percentage error

between the experimental and predicted results is found to be less than 5%, with the exception for the smoke result.

Overall, the Moringa Oleifera based biodiesel blend can be considered as a suitable and practicable biodiesel fuel for operating in diesel engine. Besides, it can be inferred that RSM is an effective optimization approach for obtaining optimum fuel injection parameter settings. With that, a more explicit understanding of the adaptation of MB50 fuel in diesel engine can be provided for engine operation under the best possible conditions.

Author Contributions: Conceptualization, Y.H.T. and H.G.H.; methodology, Y.H.T., H.G.H. and T.D.L.; formal analysis, Y.H.T., F.S.; resources, F.S., Y.H.T.; data curation, Y.H.T., H.G.H. and H.T.N., writing—original draft preparation, Y.H.T., F.S., H.G.H. and H.Y.; writing—review and editing, Y.H.T., H.G.H., H.C.O. and F.S.; visualization, T.D.L. and H.T.N.; supervision, Y.H.T. and H.G.H. All authors have read and agreed to the published version of the manuscript.

Funding: The authors would like to acknowledge Ministry of Higher Education of Malaysia and Universiti Sains Malaysia for the support through Fundamental Research Grant Scheme (FRGS)-203.PMEKANIK.6071444 (Title: Mechanism Study of Combustion and Formulation of Surrogate Biomass Producer Gas Using a CVCC System) and Universiti Sains Malaysia Research University (RUI) Grant Scheme-1001.PMEKANIK.8014136 (Title: Effect of Fuel Injection Strategies and Intake Air Supply Control on Performance, Emissions, and Combustion Characteristics of Diesel Engine Fueled with Biodiesel Blended Fuels).

Institutional Review Board Statement: Not applicable.

Informed Consent Statement: Not applicable.

Data Availability Statement: Not applicable.

Acknowledgments: The authors would like to acknowledge the Universiti Sains Malaysia for financial support toward this study.

Conflicts of Interest: The authors declare that they have no known competing financial interests or personal relationships that could have appeared to influence the work reported in this paper.

Nomenclature

ANOVA	Analysis of variances
ASTM	American society for testing and materials
BSFC	Brake specific fuel consumption
BTDC	Before top dead centre
BTE	Brake thermal efficiency
CCD	Central composite design
CO	Carbon monoxide
CV	Coefficient of variation
ECU	Engine control unit
FAME	Fatty acid methyl ester
FIP	Fuel injection pressures
F-test	Fisher's test
HC	Unburned hydrocarbon
HRR	Heat release rate
MB	Moringa oil biodiesel
MB50	50% biodiesel, 50% petroleum diesel
NO_x	Nitrogen oxides
p-value	Probability of error value
R^2	Coefficients of determination
rpm	Revolution per minute
RSM	Response surface methodology
SOI	Start of injection

References

1. Caliskan, H. Environmental and enviroeconomic researches on diesel engines with diesel and biodiesel fuels. *J. Clean. Prod.* **2017**, *154*, 125–129. [CrossRef]
2. Naderipour, A.; Abdul-Malek, Z.; Ahmad, N.A.; Kamyab, H.; Ashokkumar, V.; Ngamcharussrivichai, C.; Chelliapan, S. Effect of COVID-19 virus on reducing GHG emission and increasing energy generated by renewable energy sources: A brief study in Malaysian context. *Environ. Technol. Innov.* **2020**, *20*, 101151. [CrossRef]
3. International Energy Agency. Global Energy Review 2020. 2020. Available online: https://www.iea.org/reports/global-energy-review-2020 (accessed on 9 April 2021).
4. Mosarof, M.H.; Kalam, M.A.; Masjuki, H.H.; Alabdulkarem, A.; Ashraful, A.M.; Arslan, A.; Rashedul, H.K.; Monirul, I.M. Optimization of performance, emission, friction and wear characteristics of palm and *Calophyllum inophyllum* biodiesel blends. *Energy Convers. Manag.* **2016**, *118*, 119–134. [CrossRef]
5. Ganjehkaviri, A.; Mohd Jaafar, M.N.; Hosseini, S.E.; Musthafa, A.B. Performance evaluation of palm oil-based biodiesel combustion in an oil burner. *Energies* **2016**, *9*, 97. [CrossRef]
6. Rahman, S.M.A.; Masjuki, H.H.; Kalam, M.A.; Abedin, M.J.; Sanjid, A.; Rahman, M.M. Assessing idling effects on a compression ignition engine fueled with Jatropha and Palm biodiesel blends. *Renew. Energy* **2014**, *68*, 644–650. [CrossRef]
7. Mohd, Z.; Mohit, V.; Sarma, A.K. Biodiesel Production from Moringa oleifera Oil and Its Characteristics as Fuel in a Diesel Engine. In *Springer Proceedings in Energy, Proceedings of the First International Conference on Recent Advances in Bioenergy Research, Kapurthala, India, 25–28 February 2015*; Springer: New Delhi, India, 2016; pp. 149–157.
8. How, H.G.; Hwang, J.W.S.; Teoh, Y.H.; Chuah, H.G.; Yeoh, J.J.J.; Teh, J.S. Investigation of the Corrosion Metals in Moringa Biodiesel Fuel. *J. Adv. Res. Fluid Mech. Therm. Sci.* **2020**, *75*, 94–103.
9. Fernandes, D.M.; Sousa, R.M.F.; De Oliveira, A.; Morais, S.A.L.; Richter, E.M.; Muñoz, R.A.A. *Moringa oleifera:* A potential source for production of biodiesel and antioxidant additives. *Fuel* **2015**, *146*, 75–80. [CrossRef]
10. Atabani, A.E.; Silitonga, A.S.; Ong, H.C.; Mahlia, T.M.I.; Masjuki, H.H.; Badruddin, I.A.; Fayaz, H. Non-edible vegetable oils: A critical evaluation of oil extraction, fatty acid compositions, biodiesel production, characteristics, engine performance and emissions production. *Renew. Sustain. Energy Rev.* **2013**, *18*, 211–245. [CrossRef]
11. Abdulkareem, A.S.; Uthman, H.; Afolabi, A.S.; Awenebe, O.L. *Extraction and Optimization of Oil from Moringa oleifera Seed as an Alternative Feedstock for the Production of Biodiesel*; InTech: London, UK, 2011.
12. Esmaeili, H.; Yeganeh, G.; Esmaeilzadeh, F. Optimization of biodiesel production from *Moringa oleifera* seeds oil in the presence of nano-MgO using Taguchi method. *Int. Nano Lett.* **2019**, *9*, 257–263. [CrossRef]
13. Tüccar, G.; Uludamar, E. Emission and engine performance analysis of a diesel engine using hydrogen enriched pomegranate seed oil biodiesel. *Int. J. Hydrog. Energy* **2018**, *43*, 18014–18019. [CrossRef]
14. Arumugam, A.; Ponnusami, V. Biodiesel production from *Calophyllum inophyllum* oil a potential non-edible feedstock: An. overview. *Renew. Energy* **2019**, *131*, 459–471. [CrossRef]
15. Mahmudul, H.; Hagos, F.; Mamat, R.; Adam, A.A.; Ishak, W.; Alenezi, R. Production, characterization and performance of biodiesel as an alternative fuel in diesel engines—A review. *Renew. Sustain. Energy Rev.* **2017**, *72*, 497–509. [CrossRef]
16. Ali, O.; Mamat, R.; Rasul, M.; Najafi, G. Potential of Biodiesel as Fuel for Diesel Engine. In *Clean Energy for Sustainable Development*; Elsevier: Amsterdam, The Netherlands, 2017; pp. 557–590.
17. Noor, C.M.; Noor, M.; Mamat, R. Biodiesel as alternative fuel for marine diesel engine applications: A review. *Renew. Sustain. Energy Rev.* **2018**, *94*, 127–142. [CrossRef]
18. Teoh, Y.H.; How, H.G.; Masjuki, H.H.; Nguyen, H.-T.; Kalam, M.; Alabdulkarem, A. Investigation on particulate emissions and combustion characteristics of a common-rail diesel engine fueled with *Moringa oleifera* biodiesel-diesel blends. *Renew. Energy* **2019**, *136*, 521–534. [CrossRef]
19. Geng, L.; Xiao, Y.; Li, S.; Chen, H.; Chen, X. Effects of injection timing and rail pressure on particulate size-number distribution of a common rail DI engine fueled with fischer-tropsch diesel synthesized from coal. *J. Energy Inst.* **2021**, *95*, 219–230. [CrossRef]
20. Chen, H.; Xie, B.; Ma, J.; Chen, Y. NOx emission of biodiesel compared to diesel: Higher or lower? *Appl. Therm. Eng.* **2018**, *137*, 584–593. [CrossRef]
21. Mofijur, M.; Masjuki, H.H.; Kalam, M.A.; Atabani, A.E.; Fattah, I.M.R.; Mobarak, H.M. Comparative evaluation of performance and emission characteristics of *Moringa oleifera* and Palm oil based biodiesel in a diesel engine. *Ind. Crop. Prod.* **2014**, *53*, 78–84. [CrossRef]
22. Rashid, U.; Anwar, F.; Moser, B.R.; Knothe, G. *Moringa oleifera* oil: A possible source of biodiesel. *Bioresour. Technol.* **2008**, *99*, 8175–8179. [CrossRef]
23. Natarajan, S.; Trasy, K.A.; Srihari, N.; Raja, S. Effects of Injection Timing on CI Engine Fuelled with Algae Oil Blend with Taguchi Technique. *Energy Procedia* **2017**, *105*, 1043–1050. [CrossRef]
24. Ashok, B.; Nanthagopal, K.; Thundil Karuppa Raj, R.; Pradeep Bhasker, J.; Sakthi Vignesh, D. Influence of injection timing and exhaust gas recirculation of a *Calophyllum inophyllum* methyl ester fuelled CI engine. *Fuel Process. Technol.* **2017**, *167*, 18–30. [CrossRef]
25. Lim, G.; Lee, S.; Park, C.; Choi, Y.; Kim, C. Effect of ignition timing retard strategy on NOx reduction in hydrogen-compressed natural gas blend engine with increased compression ratio. *Int. J. Hydrog. Energy* **2014**, *39*, 2399–2408. [CrossRef]

26. How, H.G.; Masjuki, H.H.; Kalam, M.A.; Teoh, Y.H. Influence of injection timing and split injection strategies on performance, emissions, and combustion characteristics of diesel engine fueled with biodiesel blended fuels. *Fuel* **2018**, *213*, 106–114. [CrossRef]
27. Agarwal, A.K.; Srivastava, D.K.; Dhar, A.; Maurya, R.K.; Shukla, P.C.; Singh, A.P. Effect of fuel injection timing and pressure on combustion, emissions and performance characteristics of a single cylinder diesel engine. *Fuel* **2013**, *111*, 374–383. [CrossRef]
28. Mäkelä, M. Experimental design and response surface methodology in energy applications: A tutorial review. *Energy Convers. Manag.* **2017**, *151*, 630–640. [CrossRef]
29. Wang, G.; Deng, Y.; Xu, X.; He, X.; Zhao, Y.; Zou, Y.; Liu, Z.; Yue, J. Optimization of air jet impingement drying of okara using response surface methodology. *Food Control* **2016**, *59*, 743–749. [CrossRef]
30. Bezerra, M.A.; Santelli, R.E.; Oliveira, E.P.; Villar, L.S.; Escaleira, L.A. Response surface methodology (RSM) as a tool for optimization in analytical chemistry. *Talanta* **2008**, *76*, 965–977. [CrossRef]
31. Gunst, R.F. Response Surface Methodology: Process and Product Optimization Using Designed Experiments. *Technometrics* **1996**, *38*, 284–286.
32. Singh, Y.; Sharma, A.; Kumar Singh, G.; Singla, A.; Kumar Singh, N. Optimization of performance and emission parameters of direct injection diesel engine fuelled with pongamia methyl esters-response surface methodology approach. *Ind. Crop. Prod.* **2018**, *126*, 218–226. [CrossRef]
33. Montgomery, D.C. *Design and Analysis of Experiments*; John Wiley & Sons: Hoboken, NJ, USA, 2008.
34. Teoh, Y.H.; Masjuki, H.H.; Kalam, M.A.; Amalina, M.A.; How, H.G. Effects of Jatropha biodiesel on the performance, emissions, and combustion of a converted common-rail diesel engine. *RSC Adv.* **2014**, *4*, 50739–50751. [CrossRef]
35. Ghojel, J.; Honnery, D. Heat release model for the combustion of diesel oil emulsions in DI diesel engines. *Appl. Therm. Eng.* **2005**, *25*, 2072–2085. [CrossRef]
36. Mohibbe Azam, M.; Waris, A.; Nahar, N. Prospects and potential of fatty acid methyl esters of some non-traditional seed oils for use as biodiesel in India. *Biomass Bioenergy* **2005**, *29*, 293–302. [CrossRef]
37. Kumar, A.; Sharma, S. Potential non-edible oil resources as biodiesel feedstock: An. Indian perspective. *Renew. Sustain. Energy Rev.* **2011**, *15*, 1791–1800. [CrossRef]
38. Serrano, M.; Oliveros, R.; Sánchez, M.; Moraschini, A.; Martínez, M.; Aracil, J. Influence of blending vegetable oil methyl esters on biodiesel fuel properties: Oxidative stability and cold flow properties. *Energy* **2013**, *65*, 109–115. [CrossRef]
39. Pinzi, S.; Garcia, I.; Lopez-Gimenez, F.; Luque de Castro, M.; Dorado, G.; Dorado, M. The ideal vegetable oil-based biodiesel composition: A review of social, economical and technical implications. *Energy Fuels* **2009**, *23*, 2325–2341. [CrossRef]
40. Giakoumis, E.G. A statistical investigation of biodiesel physical and chemical properties, and their correlation with the degree of unsaturation. *Renew. Energy* **2013**, *50*, 858–878.
41. Heywood, J.B. *Internal Combustion Engine Fundamentals*; McGraw-Hill International: New York, NY, USA, 1988.
42. Canakci, M.; Ozsezen, A.N.; Arcaklioglu, E.; Erdil, A. Prediction of performance and exhaust emissions of a diesel engine fueled with biodiesel produced from waste frying palm oil. *Expert Syst. Appl.* **2009**, *36*, 9268–9280. [CrossRef]
43. Chauhan, B.S.; Kumar, N.; Cho, H.M. A study on the performance and emission of a diesel engine fueled with Jatropha biodiesel oil and its blends. *Energy* **2012**, *37*, 616–622. [CrossRef]
44. Szybist, J.P.; Boehman, A.L.; Taylor, J.D.; McCormick, R.L. Evaluation of formulation strategies to eliminate the biodiesel NOx effect. *Fuel Process. Technol.* **2005**, *86*, 1109–1126. [CrossRef]
45. Kwanchareon, P.; Luengnaruemitchai, A.; Jai-In, S. Solubility of a diesel-biodiesel-ethanol blend, its fuel properties, and its emission characteristics from diesel engine. *Fuel* **2007**, *86*, 1053–1061. [CrossRef]
46. Tan, P.-q.; Hu, Z.-y.; Lou, D.-m.; Li, Z.-j. Exhaust emissions from a light-duty diesel engine with Jatropha biodiesel fuel. *Energy* **2012**, *39*, 356–362. [CrossRef]
47. Saravanan, S.; Nagarajan, G.; Lakshmi Narayana Rao, G.; Sampath, S. Combustion characteristics of a stationary diesel engine fuelled with a blend of crude rice bran oil methyl ester and diesel. *Energy* **2010**, *35*, 94–100. [CrossRef]
48. Palash, S.M.; Kalam, M.A.; Masjuki, H.H.; Masum, B.M.; Rizwanul Fattah, I.M.; Mofijur, M. Impacts of biodiesel combustion on NOx emissions and their reduction approaches. *Renew. Sustain. Energy Rev.* **2013**, *23*, 473–490. [CrossRef]
49. Sharon, H.; Karuppasamy, K.; Soban Kumar, D.R.; Sundaresan, A. A test on DI diesel engine fueled with methyl esters of used palm oil. *Renew. Energy* **2012**, *47*, 160–166. [CrossRef]
50. Cheng, A.; Upatnieks, A.; Mueller, C. Investigation of the impact of biodiesel fuelling on NOx emissions using an optical direct injection diesel engine. *Int. J. Engine Res.* **2006**, *7*, 297–318. [CrossRef]
51. Shuit, S.H.; Lee, K.T.; Kamaruddin, A.H.; Yusup, S. Reactive Extraction of *Jatropha curcas*L. Seed for Production of Biodiesel: Process Optimization Study. *Environ. Sci. Technol.* **2010**, *44*, 4361–4367.
52. Chen, X.; Du, W.; Liu, D. Response surface optimization of biocatalytic biodiesel production with acid oil. *Biochem. Eng. J.* **2008**, *40*, 423–429. [CrossRef]